Journal of Magnetic Resonance 212 (2011) 386–393

Contents lists available at SciVerse ScienceDirect

Journal of Magnetic Resonance

journal homepage: www.elsevier.com/locate/jmr

Magnetic field anisotropy based MR tractography

S.H. Han [a,1], Y.K. Song [b,1], F.H. Cho [c], S. Ryu [a], G. Cho [b], Y.-Q. Song [d], H. Cho [a,*]

[a] School of Nano-BioScience and Chemical Engineering, Ulsan National Institute of Science and Technology, Ulsan, Republic of Korea
[b] Korea Basic Science Institute, Ochang, Republic of Korea
[c] Department of Physics and Astronomy, University of Southern California, Los Angeles, CA 90089, USA
[d] Schlumberger-Doll Research, One Hampshire Street, Cambridge, MA, USA

ARTICLE INFO

Article history:
Received 17 April 2011
Revised 19 July 2011
Available online 6 August 2011

Keywords:
Vessel orientation imaging
Susceptibility-induced magnetic field
Internal gradient
Diffusion

ABSTRACT

Non-invasive measurements of structural orientation provide unique information regarding the connectivity and functionality of fiber materials. In the present study, we use a capillary model to demonstrate that the direction of fiber structure can be obtained from susceptibility-induced magnetic field anisotropy. The interference pattern between internal and external magnetic field gradients carries the signature of the underlying anisotropic structure and can be measured by MRI-based water diffusion measurements. Through both numerical simulation and experiments, we found that this technique can determine the capillary orientation within 3°. Therefore, susceptibility-induced magnetic field anisotropy may be useful for an alternative tractography method when diffusion anisotropy is small at higher magnetic field strength without the need to rotate the subject inside the scanner.

1. Introduction

Determinations of the fiber orientation in biological tissue, such as the fiber pathways of brain white matter and heart muscles, provide useful information regarding the connectivity and functionality of such structures. Magnetic resonance imaging (MRI) provides non-invasive high-resolution anatomical information with structural contrast that is suitable for this application. For example, diffusion tensor imaging (DTI) compares the degree of the restriction of the apparent diffusion constant (ADC) of water molecules along multiple directions to determine the tissue anisotropy of brain white matter, in a process known as tractography [1–3].

While DTI is widely-used for tractography, its application may be limited when the inherent ADC anisotropy is small, as occurs in large capillaries. Moreover, DTI may be limited at high magnetic fields, because susceptibility-induced magnetic field inhomogeneities increase and degrade the quality of the DTI signal and resolution [5,6]. Anisotropic susceptibility-induced internal magnetic fields may be an alternative means of acquiring orientation measurements at higher field strength, and their presence has been clearly demonstrated in both white matter in the central nervous system and in myocardial capillary vessels [7,8]. However, these methods may be impractical for tractography because they require re-orientation of the subject within the scanner. The primary aim of the present study was to validate, using simulations and experiments, new procedures for acquiring tractography data at high field strengths that do not require re-orientation of the subject.

In this paper, we present a stimulated echo based MRI method that utilizes magnetic field anisotropy to determine the structural orientation without the need to rotate the subject, even when the ADC values appear uniform. For example, when a sample consisting of materials of different magnetic susceptibility levels is immersed in a uniform magnetic field, the magnetic field inside the sample is known to be inhomogeneous for grain-fluid porous media [9,10] as well as for biological cells [4,6,11–13]. For a cylindrical sample such as a capillary, the magnitude and direction of this internal field is closely related to the orientation with respect to the applied field [9,10,14,18]. For example, no internal gradient exists along the direction of the long cylindrical axis. Thus, the direction of the minimum internal gradient distribution coincides with the main capillary direction. Conventional MR techniques such as spin echo sequences [15] only measure the magnitude of the field gradients and insensitive to the orientation of internal gradients. Recently, we developed an experimental method that directly measures the magnitude and the *direction* of the internal field gradient ($\vec{g}_{int}$) according to the interference effect between the applied pulsed field gradient (PFG) and $\vec{g}_{int}$ [16]. Given that the PFG can be applied along arbitrary directions, measurements with multiple projections of $\vec{g}_{int}$ along a series of PFG directions can be obtained to fully characterize the nature of this vector. As a result, the angular dependence of the internal gradient distribution can be mapped, and the direction of the minimum $\vec{g}_{int}$ can be determined from a minimum of six independent interference experiments with different directions of PFG.

* Corresponding author.
E-mail address: hjcho@unist.ac.kr (H. Cho).
[1] Both authors have contributed to this paper equally.

1090-7807/$ - see front matter © 2011 Elsevier Inc. All rights reserved.
doi:10.1016/j.jmr.2011.07.021

This paper is organized with the following specific aims. First, we analytically show that an anisotropic susceptibility-induced magnetic field gradient is present in a single capillary when there is a magnetic field component that is perpendicular to the cylindrical axis of the capillary. Second, we extend this analytical method by determining a numerical calculation for a randomly packed capillary model for the complete mapping of angular dependence of the internal gradient distribution in a such system. The estimates of the direction of the minimum distribution width closely coincided with the direction of long cylindrical axis of capillaries, using an analogous method used to conventional DTI. Third, we experimentally obtained the interference patterns between the internal and external field gradients using a stimulated echo based MRI method with a randomly packed capillary system. This was done to show that the anisotropic distribution of the internal gradient can be experimentally obtained, and that the direction of the cylindrical axis can be obtained without the need to rotate the sample. Finally, we confirmed the sensitivity of the proposed tractography for the case when the spatial resolution is insufficient to resolve the pore structure fully, so that only the internal gradients distribution can be measured within a image voxel. As a result, we found through theoretical and experiment demonstration that this method is indeed feasible to determine the capillary orientation without sample rotation.

2. Materials and methods

For the direct visualization of the anisotropic susceptibility magnetic field contrast used in this study, we consider the susceptibility-induced internal field gradient for a single capillary tube in the presence of a B_0 field perpendicular to the cylindrical axis, as illustrated in Fig. 1A. The analytic solution of the internal field gradient outside the coaxial tube can be written as [17,18],

$$g_{int}^{x} \simeq B_0 \Delta\chi (a^2 - b^2) x \frac{x^2 - 3y^2}{(x^2 + y^2)^3} \tag{1}$$

$$g_{int}^{y} \simeq -B_0 \Delta\chi (a^2 - b^2) y \frac{y^2 - 3x^2}{(x^2 + y^2)^3} \tag{2}$$

$$g_{int}^{z} = 0 \tag{3}$$

where g_{int}^{x}, g_{int}^{y} and g_{int}^{z} is the internal gradient strength due to the volume susceptibility difference ($\Delta\chi = \chi_{tube} - \chi_{ext}$) along the x, y and z directions, respectively. B_0 is the field perpendicular to the cylindrical axis of the capillary and a and b correspond to the inner and outer radius of the coaxial tube. Fig. 1B shows the strength of internal magnetic field when $B_0 = 4.7$ T (along the x direction), $\chi_{tube} = -10.66 \times 10^{-6}$, $\chi_{water} = -9.06 \times 10^{-6}$, $a = 0.575$ mm and $b = 0.775$ mm. The values of the dimensionless SI volume magnetic susceptibility used were the same as those previously reported[18,25]. Along the x and y directions, perpendicular to the long cylindrical axis, the strong gradient exists near the outside surface with opposite signs across the cylinder, and it decays as one moves away from the cylinder. A strong anisotropy is observed along the z direction because susceptibility-induced $\vec{g}_{int}$ does not exist along this direction, which is the fundamental contrast utilized in this study.

To calculate the position dependent local internal magnetic field of randomly packed glass capillaries, we first obtained the positions of all capillaries by MRI, then the contribution of magnetic field and gradient from each capillary is calculated and summed for all the capillaries. This method has been presented in detail in [24,26,29] and a brief description is given here. In this method, the boundary between the two materials (glass and water) is assigned a magnetic charge density value, $\varrho_m \propto \hat{s} \cdot \hat{x}$, where $\hat{s}$ is the local surface normal and $\hat{x}$ is the applied field direction. The total susceptibility-induced magnetic field is the linear sum of the contributions from all surfaces for small susceptibility contrasts ($\Delta\chi \ll 1$):

$$\vec{B}_x^{int}(\vec{r}) = B_0 \frac{\mu_0}{4\pi} \Delta\chi \int \frac{\vec{r} - \vec{r}'}{|\vec{r} - \vec{r}'|^3} (\hat{s}' \cdot \hat{x}) dS'. \tag{4}$$

For the numerical implementation, first, a black and white representation (1024 × 1024 voxels) of cylinders was created from the measured spin density image at $t_d = 50$ ms to obtain a high resolution replica of the experimental setup of the capillary model. The image was placed at the center of a 2048 × 2048 area to remove any boundary effect. The susceptibility-induced magnetic field with given an external field direction was calculated by superposition of the dipole field from each voxel of the solid (glass) taken as a point source [26,29]. This linearized approach has been used widely previously [19–23] to calculate local fields and has been shown to accurately reproduce the analytical results of cylindrical models[24] and also validated using experimental measurements of internal gradient with randomly packed capillary tubes[16] . The angle-resolved gradients $\vec{g}_{int} \cdot \hat{n}$ (where $\hat{n}$ is the unit vector along the arbitrary direction) were then evaluated on the image grid and the distribution of the angle-resolved gradients was obtained along each direction.

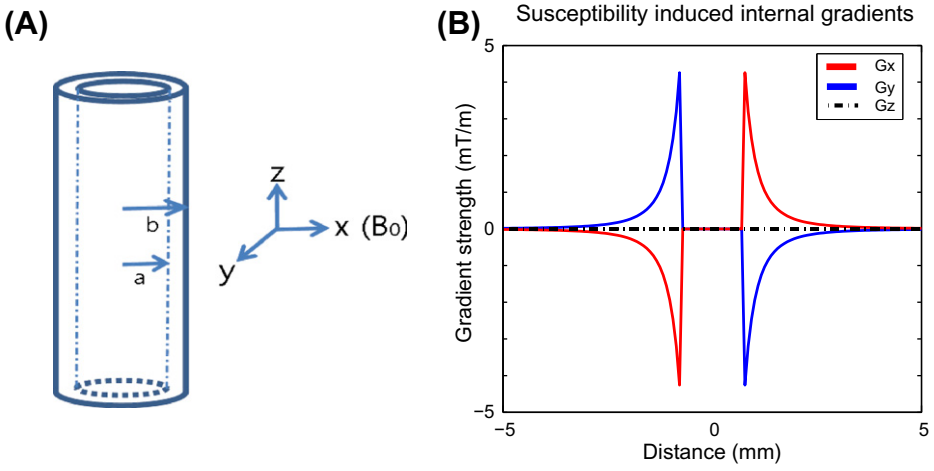

Fig. 1. (B) plots the susceptibility-induced magnetic field gradient for a capillary tube along three (x, y and z) different directions. The cylinder is aligned along the z direction, perpendicular to the direction of B_0 field (x) as sketched in (A). The annular field of coaxial tube was set to zero as it produces no NMR signal.

In a randomly packed capillary model, the profile of the internal gradients becomes complex and heterogeneous depending on the local packing configuration [16,24,27]. For example, Fig. 2A–D illustrate the components of $\vec{g}_{int}$ along the [100], [101], [010] and [011] directions, respectively, Moreover, these figures also show the corresponding histogram distribution for each direction. The direction of the B_0 (x axis) was perpendicular to the cylindrical axis of capillaries. The histograms of the angle-resolved gradient distributions are shown to be symmetric about zero for a randomly packed capillary model. Thus, the corresponding width of each distribution was estimated. The values of the normalized widths with respect to the [100] direction are shown on the onset of each distribution. Narrower distributions were observed along the [101] and [011] directions compared to those along [100] and [010] directions and this reflects the fact that no internal gradient exists along the [001] direction, which is the direction of the cylindrical axis of capillaries. Fig. 2E shows the widths of the angle-resolved gradient distributions along an arbitrary direction in Cartesian coordinates for the randomly packed capillary model and the complete angular dependence of the internal gradient distribution. The distance of the particular surface point of the oblate shape from the origin represents the width of the angle-resolved gradient distribution along the corresponding direction. Given that $\vec{g}_{int} \cdot \hat{z} = 0$, the oblate shape converges to zero along the z direction. Fig. 2F shows the corresponding width anisotropy when the capillaries are rotated 20° around the x direction and shows the sensitivity of the shape at the oblique angles.

The ellipsoidal geometry of the width of the angle-resolved internal gradient distribution reflects the alignment of capillaries along the direction of minimum width for an oblate geometry. It is well known that six parameters are needed to define an ellipsoidal geometry, three eigenvectors that are perpendicular to each other and three associated eigenvalues that determine the lengths of eigenvectors. Six independent measurements of the distribution widths along different directions are sufficient to determine the width ellipsoid, whose eigenvector and eigenvalues describe the directions and the lengths of the principal axes, respectively. The eigenvector with the minimum eigenvalue then corresponds to the direction of main capillaries.

To determine the six parameters of the width ellipsoids from six independent measurements, the procedure described was followed. First, a symmetric 3 by 3 matrix W was defined to be [2]

$$W = \begin{bmatrix} W_{xx} & W_{xy} & W_{xz} \\ W_{yx} & W_{yy} & W_{yz} \\ W_{zx} & W_{zy} & W_{zz} \end{bmatrix}. \quad (5)$$

This internal gradient width tensor W is a symmetric tensor, which means $W_{ij} = W_{ji}$. When the width ellipsoid is aligned in Cartesian coordinates, the off-diagonal terms of W are zero. When

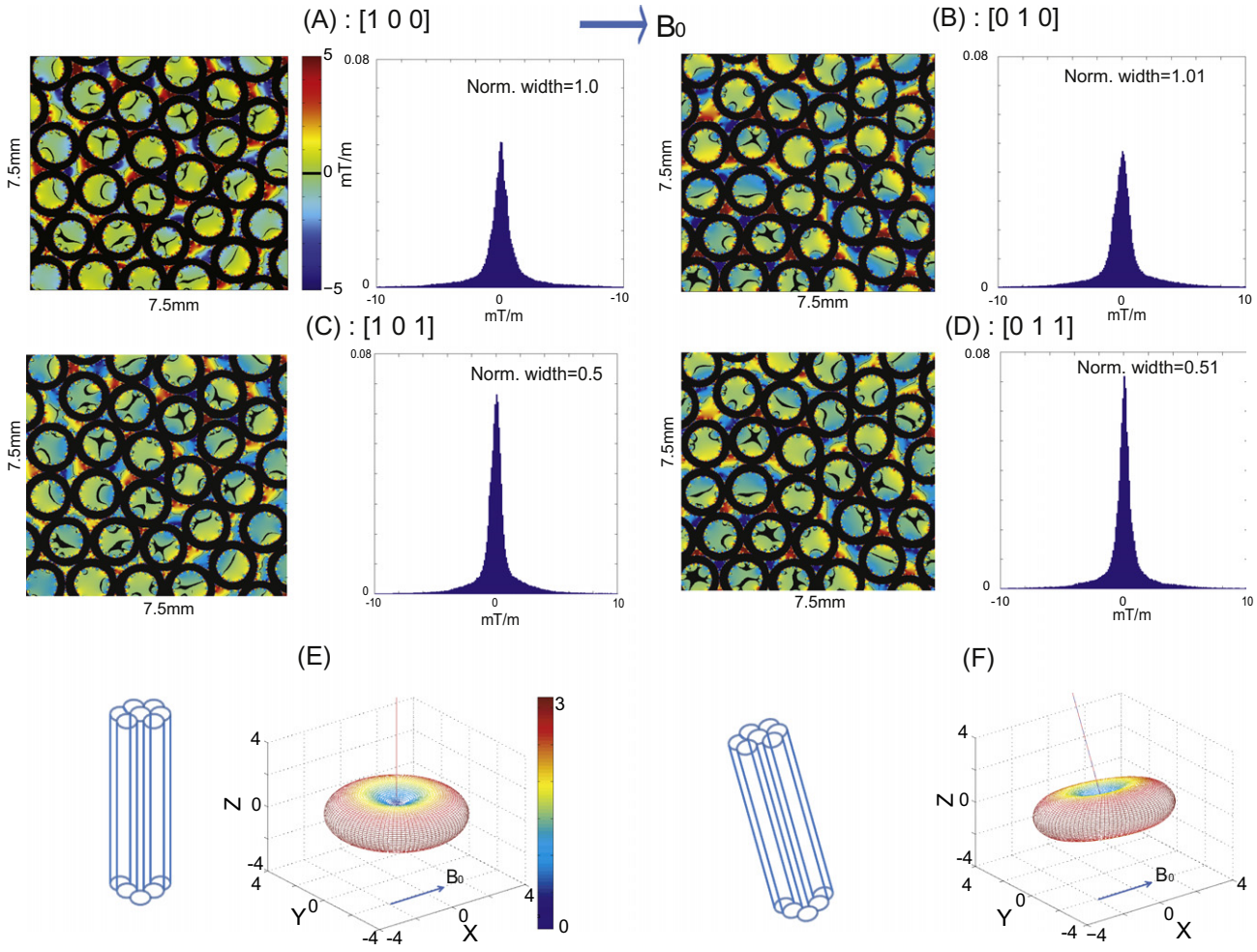

Fig. 2. (A)–(D) visualize the components of $\vec{g}_{int}$ along the [100], [101], [010] and [011] directions, respectively and a corresponding histogram distribution for each direction is shown. (E) Plots the widths of angle-resolved gradient distributions along an arbitrary direction in the Cartesian coordinate for the randomly packed capillary model and shows the complete angular dependence of internal gradient distribution. (F) Plots the corresponding width anisotropy when the capillaries are rotated 20° around the x.

they are not aligned, the off-diagonal terms are non-zero and diagonalization of W gives three eigenvalues and eigenvectors, whose minimum values coincide with the direction of the cylindrical axis of the capillaries.

Analogous to conventional DTI method of obtaining diffusion tensors, width tensors W are determined from six independent measurements using the below equation,

$$\hat{n}^T \cdot W \cdot \hat{n} = \mathrm{var}(H_n) \tag{6}$$

where $\hat{n}$ is the unit vector along which the distribution is measured, H_n is the distribution along the direction of $\hat{n}$, and var(H_n) refers to the variance of the distribution (H_n). The six parameters for the width tensor were determined from six independent width measurements along the directions of $[n_x, n_y, n_z] = [1\,1\,0]$, $[-1\,1\,0]$, $[0\,1\,-1]$, $[0\,-1\,-1]$, $[1\,0\,-1]$, $[-1\,0\,-1]$. After the measurements were obtained, the inverse of the below equation was used to obtain the six parameters of W:

$$W_{xx}n_x^2 + W_{yy}n_y^2 + W_{zz}n_x^2 + 2W_{xy}n_xn_y + 2W_{xz}n_xn_z + 2W_{yz}n_yn_z = \mathrm{var}(H_n). \tag{7}$$

After the determination of W, a matrix diagonalization was followed to determine the direction of the minimum eigenvalue, which coincides with the direction of cylindrical axis of the capillaries. The data were processed using MATLAB R2010a (MathWorks, Natick, MA) and the outline of this procedure is presented in the Appendix.

Fig. 3 summarizes the determinations of the direction of the cylindrical axis at oblique angles using the W tensor approach with numerical calculations of internal gradient of randomly packed capillaries. Fig. 3A presents a comparison of the direction of the cylindrical axis and the minimum eigenvalue direction of the W tensor, which shows excellent agreement for both the rotation of cylindrical pack toward the direction of the B_0 field (y rotation) and the rotation around the direction of the B_0 field (x rotation). Fig. 3B shows the change in the maximum eigenvalue for x and y rotation, respectively. During the y rotation, the magnitude of the susceptibility-induced gradient decreases in proportion to the magnitude of decrease in the strength of the B_0 component that is perpendicular to the cylindrical axis. Although, this is expected to lead to reduced contrast (finally disappearing when perfectly aligned with B_0) and the measured decreases in the maximum eigenvalues of the W tensor is consistent with this possibility, but the minimum width of the gradient distribution was still along the cylindrical axis.

The value of $\vec{g}_{int}$ can be uniquely determined in experiments using the pulsed gradient stimulated echoes from diffusing spins. Using this data, the magnetic field anisotropy of the capillaries can be experimentally measured. To validate this procedure, a stimulated echo-based ($\pi/2 - t_e - \pi/2 - t_d - \pi/2 - t_e -$ echo) spin-warp imaging sequence was employed [10,28]. This imaging method modulates the spin magnetization with internal gradients during the encoding time (t_e) and records the decay of the magnetization as a function of the diffusion time (t_d). The decay of the stimulated echo was measured at a series of diffusion times and the decay rates of the echo signal were measured according to the model. These are written as $1/T_{eff} = 1/T_b + \gamma^2 t_e^2 D g_{int}^2$, where $1/T_b$, γ, t_e and D represent the background decay rates (such as T_1), the magnetogyric ratio, the encoding time and the diffusion constant, respectively. Previous research showed that the strength of internal gradients (g_{int}^2) measured with this method was in excellent agreement with the theoretical calculations of the internal gradient. However, any orientation information is lost using this method because only the squared magnitude is measured. To retrieve the orientation of the internal gradient, an external field gradient $\vec{g}_{ext}$ was applied during the encoding time to generate the cross-term between the external and internal gradients, $\vec{g}_{ext} \cdot \vec{g}_{int}$. This allowed for the determinations of the decay rate from the total gradient, $\vec{g}_{total} \equiv \vec{g}_{ext} + \vec{g}_{int}$, $1/T_{eff} = 1/T_b + \gamma^2 t_e^2 D g_{total}^2$, where $g_{total}^2 = g_{int}^2 + g_{ext}^2 + 2\vec{g}_{ext} \cdot \vec{g}_{int}$ containing the cross-term. As the direction and magnitude of $\vec{g}_{ext}$ can be controlled, the full vector property of $\vec{g}_{int}$ can be mapped and the width of the internal gradient distribution along any direction can therefore be measured. The sample consisted of randomly packed glass capillaries (Fisherbrand) with an inner diameter of 1.15 mm and a wall thickness 0.2 mm that were filled with distilled water both inside and between the capillaries. The cylindrical pack was 24 mm long with a 15 mm radius including ~30 capillaries. Capillaries were randomly packed into the machined plastic holder as shown in the inset of Fig. 4F. After filling the capillaries with water and sealing them, the bottom of the holder was glued to the end of a flat wooden stick and centered inside a commercial birdcage MRI volume coil (Bruker Biospin, Billerica, MA). The direction of the cylindrical axis was aligned with the MR images until the desired orientation was set to the z direction. The rotation around the x axis (B_0 direction) was achieved by rotating the entire probe around x direction. For the y rotation, the angled wedge was placed and glued between the sample holder and wooden stick to align the sample toward the B_0 direction at the desired angle. The susceptibility difference between the glass and water gives rise to an internal gradient of approximately 4 mT/m near the surface for a single cylinder. This gradient and

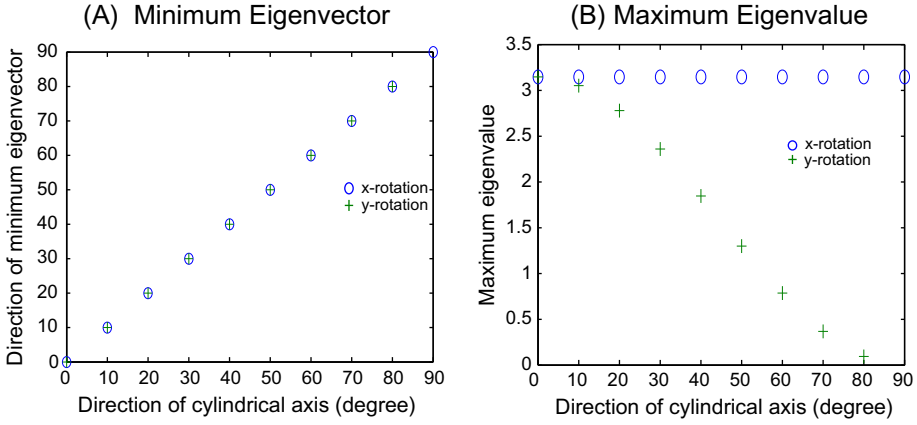

Fig. 3. (A) compares the direction of the cylindrical axis and the minimum eigenvalue direction of W tensor, which shows excellent agreement for both rotation of cylindrical pack toward the direction of the B_0 field (y rotation) and around the direction B_0 field (x rotation). (B) Shows the change of maximum eigenvalue for x and y rotation, respectively.

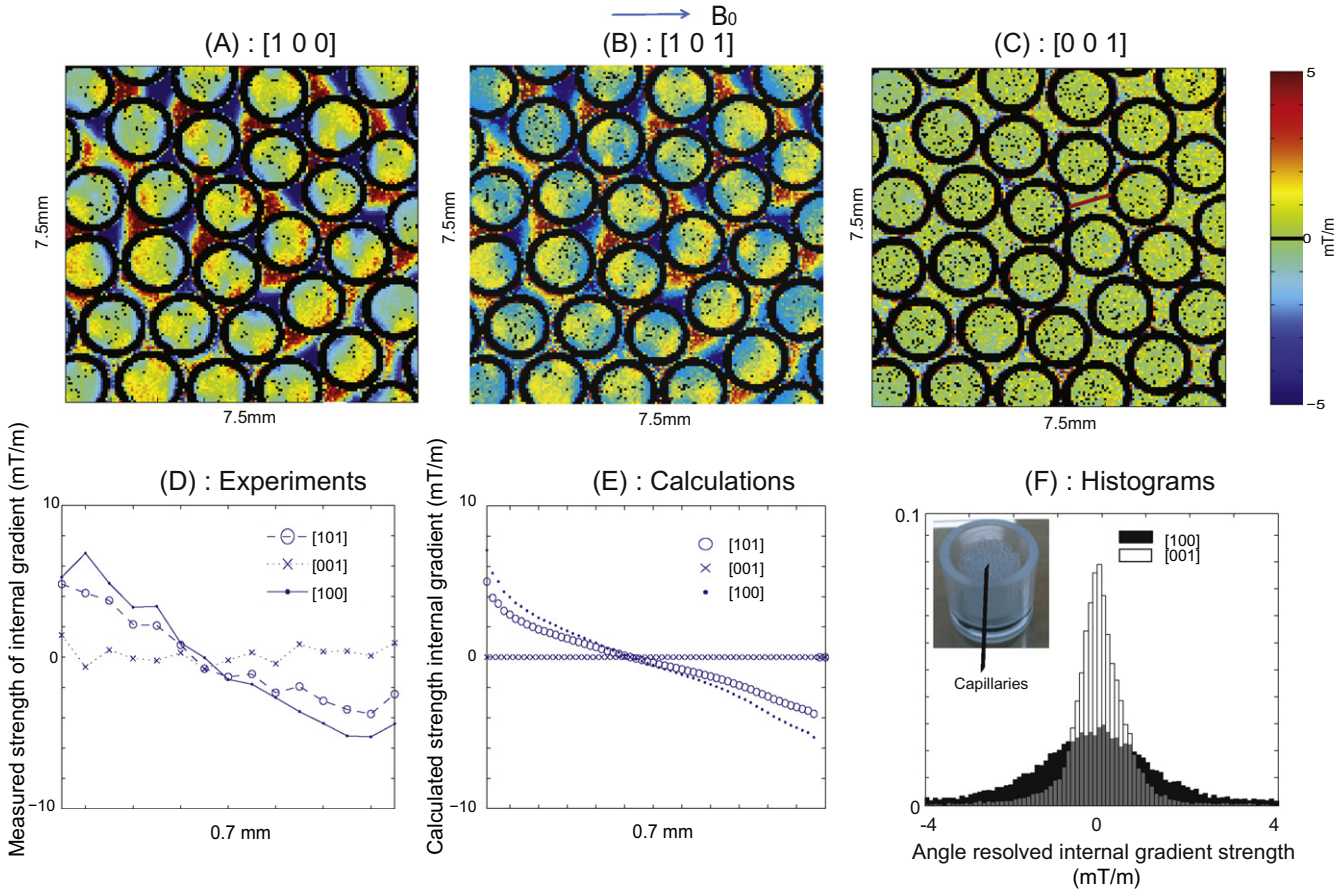

Fig. 4. (A)–(C) show the strength of the experimentally measured internal gradients along three different directions. (D) and (E) Compare the line intensities of measured internal gradient strength with that of numerical calculations along the line segment shown in C for three different orientations. (F) Overlays both the histogram distribution of the internal gradients along the *x* (A) and *z* (C) directions, respectively.

the internal field calculations are shown in Fig. 1B for a 4.7-T NMR system (Bruker Biospin, Billerica, MA).

3. Experimental results

In initial experiments, the simulation parameters were compared to experimental measurements of the internal gradient using stimulated echo sequence. The measured decay rate due to diffusion inside internal gradient for the image voxel close to the surface of one of the capillaries and was 2.9 (1/s). This decay rate was converted to the strength of internal gradient using $1/T_{int} = \gamma^2 t_e^2 D g_{int}^2$ to obtain 3.8 mT/m (t_e = 40 ms, D = 1.8 × 10^{-5} cm^2/s). The experimentally measured internal gradient values were similar to the values from the calculation shown in Fig. 1B.

Next, the individual decay rates for three different orientations ([100], [101], [001]) of $\vec{g}_{ext}$ were measured, and the terms $\vec{g}_{ext} \cdot \vec{g}_{int}$ are presented in Fig. 4A–C. The applied external gradient pulse was 5 mT/m and 35 ms long during the encoding time of the three different directions. The diffusion constants were measured and found to be identical in the capillary-free region of the samples along different directions. The total encoding time was 70 ms. The diffusion time was varied sequentially from 50 to 500 ms and the corresponding decay rates were evaluated by exponential

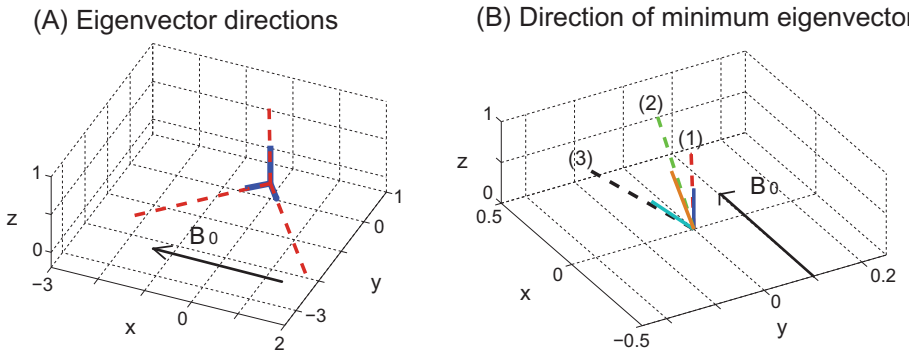

Fig. 5. In (A), the dotted lines plot the directions of the three principal eigenvectors estimated from the experimental measurements along with the expected principal axes of the capillary pack (solid lines). (B) Compares the direction of the measured *minimum* eigenvalues (dotted lines) with the expected (solid lines) orientation of the capillary pack at oblique angles with respect to the B_0 magnetic field. (0°, 10° and 20° are labeled as (1), (2) and (3), respectively).

fitting for each pixel. Each decay rate measurement was subtracted from reference experiments with $\vec{g}_{ext} = 0$ so that only the cross-term $\vec{g}_{ext} \cdot \vec{g}_{int}$ was extracted. The g^2_{ext} term, which adds a constant value to the distribution, was subtracted as well. For three different orientations, Fig. 4D and E compare the line intensities of the measured internal gradient strength with that of the numerical calculations along the line segment shown in (C). Consistent with the simulations, the strength of the angle-resolved internal gradient was the strongest along the [100] direction. Fig. 4F plots the corresponding histogram of the $\vec{g}_{int}$ distribution along the x ([100]) and z ([001]) directions and, as expected, shows a narrower distribution along the z direction. An imperfect alignment of the cylinders is likely to give rise to some extent of the z component of $\vec{g}_{int}$, as shown by the trigonal pore in the above figure, where the internal gradient is relatively strong.

With the same configuration, the measurements were repeated for the six different orientations ([110], [−110], [01−1], [0−1−1], [10−1], [−10−1]) of $\vec{g}_{ext}$ to obtain the corresponding width of the distribution of each direction. A series of experiments was repeated with three different random cylinder packing to determine the reproducibility of the technique. From these measurements, the width tensor W was obtained by inverting Eq. (7). Subsequently, matrix diagonalization was followed to find the minimum eigenvector direction. Fig. 5A shows a comparison between the three eigenvectors derived from the these measurements (dotted lines) superimposed on the principal axes of the capillaries, where z is the direction of the long cylindrical axis. In all cases, the direction of the minimum eigenvector determined the direction of the long cylindrical axis within 3° with all eigenvectors orthogonal to each other. As there is no preferred directions of two of the eigenvectors on the x–y plane, one eigenvector of W tensor was aligned with one of the dotted lines on the x–y plane.

To test the method in the case of oblique angles, two additional experiments were performed. In the first experiment, the capillary pack was rotated 20° around the y axis, while the magnetic field was maintained along the x direction. Measurements for the six different orientations with reference experiments were conducted, and the corresponding direction of the minimum eigenvalues was calculated. The eigenvector with the minimum width (dotted line (3)) was found to tilt 18.2° from the [001] (z) direction around the y axis. These data and, the expected direction of the capillary (solid line (3)) are shown in Fig. 5B. In the second experiment, the capillary pack was rotated 10° around the x axis and the same experiments were repeated. The eigenvector with the minimum width (dotted line (2)) was found to tilt 11.2° from the [001] direction around the x axis. These data and the expected direction of the capillary (solid line (2)) are shown in Fig. 5B.

It is worthwhile to consider cases when the spatial resolution is insufficient to fully resolve the pore structure so that only the distributions of the internal gradients can be measured. This is particularly important for *in vivo* MRI applications. In these cases, the variation of $\vec{g}_{int}$ exists within a single image voxel, and the measured MR signal in the voxel is a weighted exponential function, $S = \Sigma_i f(g_i) e^{-t_d/T_{eff}}$, where $f(g_i)$ and T_{eff} are the weight and the total decay rates associated with the corresponding internal gradient, respectively, and t_d is the diffusion time. The value of $f(g_i)$ was estimated from the calculated internal gradient distribution along different directions, and $1/T_{eff}$ was modeled to follow the magnitude of $g^2_{int} + g^2_{ext} + 2\vec{g}_{ext} \cdot \vec{g}_{int}$ from the theoretical calculations. Fig. 6A plots the signal S, as a function of t_d and $\vec{g}_{ext}$ along the x, y and z directions, respectively. Highly non-exponential decay was observed for $\vec{g}_{ext}$ along x and y axes, where the internal gradient has a broad distribution. The signal was seen to be nearly mono-exponential for $\vec{g}_{ext}$ along the z direction, which is parallel to the cylindrical axis. Fig. 6B shows the corresponding experimental

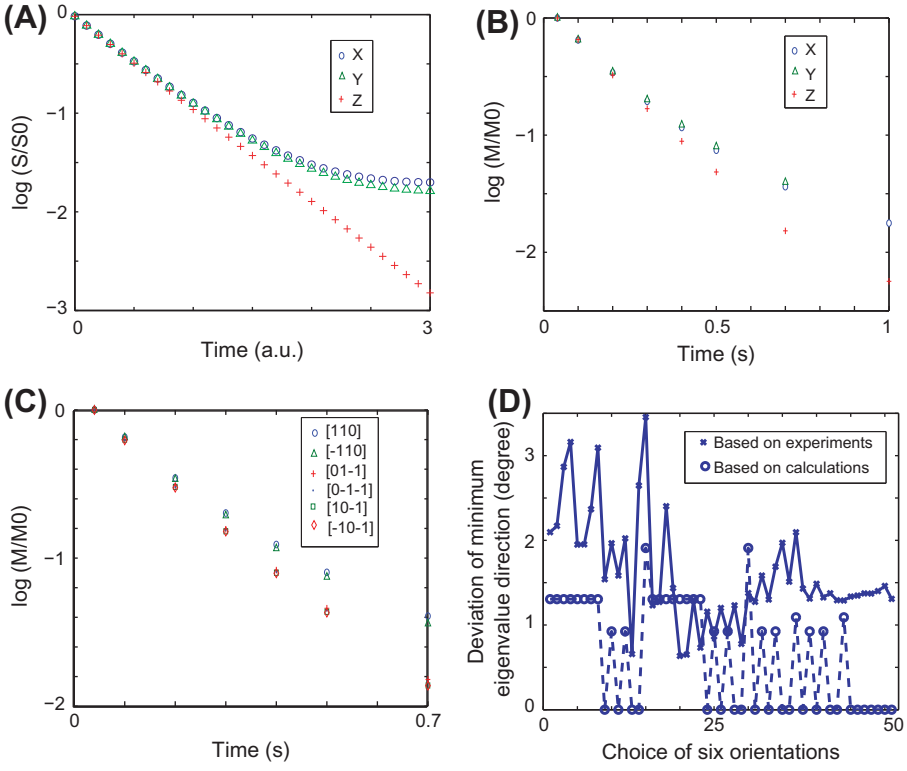

Fig. 6. (A) Plots the signal S, as a function of the diffusion time (t_d) with $\vec{g}_{ext}$ along the x, y and z directions, respectively. (B) The corresponding experimental decay of the echo signal when $\vec{g}_{ext}$ was applied along three different directions. (C) The experimental decay of the echo signal when $\vec{g}_{ext}$ for six different orientations was applied. (D) Deviation angles of the minimum eigenvalue direction from the expected direction. Both the theoretical (○) and experimental (×) deviations of the minimum eigenvalue direction for various combinations are plotted.

measurements of the decay of the magnetization for $\vec{g}_{ext}$ along x, y and z axes, showing an identical trend to the theoretical values. It is possible to use the inverse Laplace transform for each voxel to obtain the width of the internal gradient distribution along each direction followed by an eigenvector analysis to obtain the direction of the minimum eigenvalue. However, the degree of deviation from single exponential behavior is supposed to characterize the width of the underlying distribution of the internal gradient well. Thus, the difference in the signal at a particular time point along each direction can be measured in reference to that of a single exponential curve and an eigenvector analysis can be subsequently used to perform the tractography with these data.

To experimentally confirm the sensitivity of the tractography for a low-resolution signal with gradient distributions, the total signal at corresponding diffusion time was plotted for various diffusion time points for six different orientations, as shown in Fig. 6C. The direction of the cylindrical axis was along the z direction, whereas the direction of the B_0 field is along the x direction. A clear deviation from single exponential decay was observed for $\vec{g}_{ext}$ along both the [1 1 0] and [−1 1 0] directions, which shows the maximum width of the gradient distributions. Less deviation was observed for the remaining directions containing the z component of the external field gradients. To find the direction of the cylindrical axis, the deviation from the single exponential curve was estimated for each of the six directions at each time point by dividing the corresponding data with respect to the single exponential curve. The directions of the minimum eigenvalue of these ratios were then estimated at a particular time point. The direction of the minimum eigenvalue was seen to fall within 2° of the deviation from the z direction for the three representative time points.

Finally, to test the angular sampling dependence of the eigenvector determination for the six orientation measurements, nine directions ([1 1 0], [−1 1 0], [0 1 −1], [0 −1 −1], [1 0 −1], [−1 0 −1], [1 0 0], [0 1 0], [0 0 −1]) were sampled and the corresponding widths were estimated with both theoretical and experimental data. Fig. 6D summarizes both the experimental and theoretical deviation errors for the direction of the minimum eigenvalues, which was determined from the width measurements from six of the 51 combinations of directions. The condition number of the inverted matrix was less than six for all cases plotted in the figure.

4. Conclusions and discussions

In summary, we have both theoretically and experimentally demonstrated the feasibility of using a magnetic-field anisotropy-based MRI method to obtain fiber orientations in a randomly packed capillary model without the need to reorient the subject with respect to the direction of the main magnetic field. A distinct angular dependence of the internal gradient distribution was observed when the main magnetic field direction did not coincide with the direction of cylindrical axis. The widths of the resulting distribution along the six independent directions were used to estimate the *minimum* width eigenvalue and eigenvector, analogous to that of conventional DTI technique, where the maximum eigenvector of ADC was obtained for tractography. The direction of the minimum width eigenvalue of the internal gradient distribution was shown to follow the direction of the long cylindrical axis of the capillaries, demonstrating the feasibility of the proposed method as an alternative tractography method. The sensitivity of the interference contrast between internal and external gradients was also verified and an alternative data processing method is presented in the case of limited image resolution as well.

The methods developed presented in this study have two important advantages. First, these magnetic field anisotropy based methods may be sensitive to the fiber orientation, whereas the use of conventional DTI may not be possible when there are small angular variations of the ADC values for large vessels or significant susceptibility-induced magnetic field interference at higher magnetic field strength. Accordingly, the methods we have developed may become an important complement to conventional DTI in such cases. Second, recently reported susceptibility tensor imaging [7,8] methods may provide new structural in vivo contrast, but may not be practical, because they require reorientation of the subject in side the magnet. The presently described method utilizes the angular variations of the interference pattern of the internal and external gradients. As external gradient directions can be routinely rotated to obtain the desired angular contrast, the proposed method may offer a more practical way to obtain anisotropy information for fiber materials than conventional susceptibility tensor imaging methods, which require cumbersome sample rotations inside the magnet. Further validation of this method requires study of the sensitivity of the interference effect as a function of diffusion and the structural length of various system and in vivo verifications in animal model using intravascular contrast agents.

Acknowledgements

This work was supported by the National Research Foundation of Korea Grants funded by the Korean Government (Nos. 2010-0029434 and 2010-0003608), Korea Basic Science Institute (T31403) and by the support program for the advancement of national research facilities and equipment by the MEST. This work was also supported by the year of 2010 Research Fund of the UNIST.

Appendix A

Assignment of six non-colinear directions:

```
Xh = [1,−1,0,0,1,−1];
Yh = [1,1,1,−1,0,0];
Zh = [0,0,−1,−1,−1,−1];
```

Normalization:

```
for m = 1:6
X = Xh(m);
Y = Yh(m);
Z = Zh(m);
X = X./(sqrt(X.^2 + Y.^2 + Z.^2));
Y = Y./(sqrt(X.^2 + Y.^2 + Z.^2));
Z = Z./(sqrt(X.^2 + Y.^2 + Z.^2));
```

Measurement matrix along six directions:

```
M(m,:) = [X.^2, Y.^2, Z.^2, 2*X.*Y, 2*Y.*Z, 2*Z.*X];
m = m + 1;
end
```

Width vector along six directions (width1 = 3.63, width2 = 3.67, width3 = 1.56, width4 = 1.56, width5 = 1.56, width6 = 1.56):

```
W = [width1, width2, width3, width4, width5, width6]';
```

Calculation of width tensor:

```
A = inv(M)*W;
a = A(1,:);
```

17: $b = A(2,:)$;
18: $c = A(3,:)$;
19: $d = A(4,:)$;
20: $e = A(5,:)$;
21: $f = A(6,:)$;
22: $TS = [a,d,f;\ d,b,e;\ f,e,c]$;

Diagonalization:

23: $[V,D] = eig(TS)$

Angle between the minimum eigenvector and [001] (cylindrical axis) direction:

24: $VV = V(:,1)'$;
25: $C = dot(VV,[0,0,1])$;
26: $VVV = sqrt((VV(1))^2 + (VV(2))^2 + (VV(3))^2)$;
27: $ang = acos(C/VVV) * (180/pi)$

References

[1] P.T. Callaghan, S. Godefroy, B.N. Ryland, Magn. Reson. Imaging. 21 (2003) 243–248.
[2] P.J. Basser, J. Mattiello, D. LeBihan, J. Magn. Reson. 103 (1994) 247–254.
[3] S. Mori, B.J. Crain, V.P. Chacko, P.C.M. van Zijl, Ann. Neurol. 45 (1999) 265–269.
[4] P.W. Kuchel, C.J. Durrant, B.E. Chapman, P.S. Jarrett, D.G. Regan, J. Magn. Reson. 145 (2000) 291–301.
[5] P.J. Basser, D.K. Jones, NMR Biomed. 15 (2002) 456–467.
[6] S. Mori, P.C.M. van Zijl, NMR Biomed. 15 (2002) 468–480.
[7] A. Vignaud, I. Rodriguez, D.B. Ennis, R. Desilva, P. Kellman, J. Taylor, E. Bennett, H. Wen, Magn. Reson. Med. 55 (2006) 725–730.
[8] C. Liu, Magn. Reson. Med. 63 (2010) 1471–1477.
[9] R.J.S. Brown, Phys. Rev. 121 (1961) 1379.
[10] Y.-Q. Song, S. Ryu, P.N. Sen, Nature 406 (2000) 178–181.
[11] K.M. Brindle, F.F. Brown, I.D. Campbell, C. Grathwohl, P.W. Kuchel, Biochem. J. 180 (1979) 37–44.
[12] Z.H. Endre, P.W. Kuchel, B.E. Chapman, Biochim. Biophys. Acta 803 (1984) 137–144.
[13] P.W. Kuchel, B.T. Bulliman, NMR Biomed. 2 (1989) 151–160.
[14] P.W. Kuchel, B.E. Chapman, W.A. Bubb, P.E. Hansen, C.J. Durrant, M.P. Hertzberg, Concept Magn. Reson. 18A (2003) 56–71.
[15] E.L. Hahn, Phys. Rev. 80 (4) (1950) 580–594.
[16] H. Cho, S. Ryu, J.L. Ackerman, Y.-Q. Song, J. Magn. Reson. 198 (1) (2009) 88–93.
[17] R. Bhagwandien, R.V. EE, R. Beersma, C.J.G. Bakker, M.A. Moerland, J.J.W. Lagendijk, Magn. Reson. Imaging. 10 (2) (1991) 299–313.
[18] S.C.-K. Chu, Y. Xu, J.A. Balschi, C.S. Springer, Magn. Reson. Med. 13 (1990) 239–262.
[19] L.D. Landau, E.M. Lifshitz, Electrodynamics of Continuous Media, Pergamon, New York, 1960. pp. 45–47.
[20] L.E. Drain, Phys. Soc. Proc. 80 (1962) 1380.
[21] S. Majumdar, J.C. Gore, J. Magn. Reson. 78 (1988) 41.
[22] R.M. Weisskoff, C.S. Zuo, J.L. Boxerman, B.R. Rosen, Magn. Reson. Med. 31 (1994) 601.
[23] A.P. Pathak, B.D. Ward, K.M. Schmainda, Neuroimage 40 (2008) 1130–1143.
[24] P.N. Sen, S. Axelrod, J. Appl. Phys. 86 (1999) 4548–4554.
[25] R. Engel, D. Halpern, S. Bienenfeld, Anal.Chem. 45 (1973) 367.
[26] L.-S. Bouchard, W.S. Warren, J. Magn. Reson. 170 (2) (2004) 299–309.
[27] H. Cho, Y.-Q. Song, Phys. Rev. Lett. 100 (2008) 025501.
[28] N.V. Lisitza, Y.-Q. Song, Phys. Rev. B. 65 (2002) 172406.
[29] G. Deville, M. Bernier, J.M. Delrieux, Phys. Rev. B. 19 (11) (1979) 5666.